Phase diagram of microtubules

Deborah Kuchnir Fygenson, Erez Braun,* and Albert Libchaber†
Physics Department, Princeton University, Princeton, New Jersey 08544
(Received 4 April 1994)

We map the phase diagram of microtubules as a function of temperature and tubulin concentration. We observe spontaneous and site-nucleated microtubule assembly. At temperatures and concentrations below the onset of spontaneous nucleation, we measure the steady-state proportion of occupied nucleation sites and the distribution of lengths of site-nucleated microtubules. Our observations reveal a transition in the length dynamics of microtubules from bounded to unbounded growth. This transition is also evident in the length dynamics of individual site-nucleated microtubules. The transition to spontaneous microtubule assembly completes the phase diagram. We measure the temperature and concentration dependence of the latent time for spontaneous nucleation of microtubules in the bulk.

PACS number(s): 87.15.−v, 64.60.−i

I. INTRODUCTION

The protein *tubulin* is found in every cell of every living organism (with the exception of bacteria) [1]. In the presence of guanosine-tri-phosphate (GTP) and magnesium ions (Mg^{2+}), tubulin-GTP complexes form [2] and aggregate [3] into long, hollow cylinders called *microtubules.* Microtubules are about 25 nm in outer diameter, incorporate 1625 tubulin dimers per micrometer of their length [4] and easily grow long enough to span a cell (10–100 μm). In the cell, microtubules form a network that supports the overall structure and guides internal transport [5]. Fundamental cellular processes, like locomotion, morphogenesis, and reproduction, rely on the ability of microtubules to change their organization. This ability derives from a unique feature of microtubule assembly called *dynamic instability* [6].

The term dynamic instability describes the fact that individual microtubules are dynamic structures that fluctuate erratically between assembling and disassembling. These fluctuations are not microscopic; they often involve most or all of the microtubule. A typical plot of the length of a single microtubule over time is shown in Fig. 1. This so-called dynamic instability depends on the hydrolysis reaction which turns the GTP of the tubulin-GTP complex into guanosine-di-phosphate (GDP) and releases energy ($\sim 8kT$/reaction) [7].

Dynamic instability has been the subject of research for the past decade. The key element of all models is a competition between growth and the process of hydrolysis, often considered in terms of a growth front and a possible hydrolysis front. Crudely, when the hydrolysis front overtakes the growth front, the microtubule structure becomes unstable. The question of exactly how the hydrolysis and growth reactions are coupled continues to draw attention [8]. Experimental control parameters include temperature and tubulin concentration, as well as the *p*H of the solution, the presence of certain other proteins [microtubule-associated proteins (MAP's)] [9], and the concentrations of GTP and Mg^{2+} ions [10]. Of these, the most biologically relevant parameter is perhaps the concentration MAP's. However, to understand dynamic instability the concentration of tubulin has been the preferred variable, since it affects the growth velocity but not the hydrolysis of GTP.

In the work described here, we vary both temperature and tubulin concentration and map the phase diagram of microtubule growth. We study both spontaneously nucleated assembly and growth from nucleation sites [11]. The resulting phase diagram is shown in Fig. 2.

At low temperatures, microtubules only grow from nucleating sites. For a range of temperatures, a steady state is reached in which only a fraction of the sites have mi-

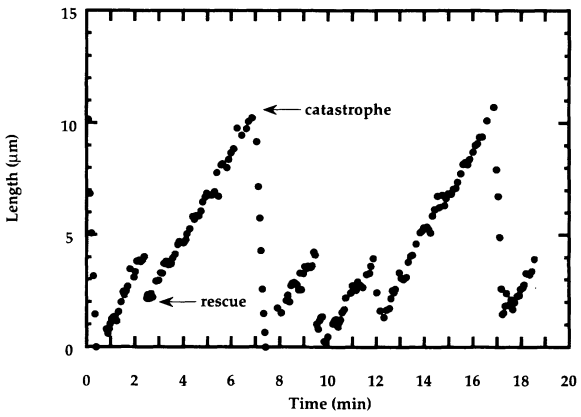

FIG. 1. A typical time series of the length of a single microtubule. The velocities of growth range between 1.6 and 2.3 μm/min (40–65 dimers/sec), while the velocities of shortening are 10 times faster. The transitions from growth to shortening are called *catastrophes;* transitions from shortening to growth are called *rescues.*

*Present address: Department of Physics, Technion, Haifa, Israel.
†Also at NEC Research Institute, 4 Independence Way, Princeton, NJ 08540.

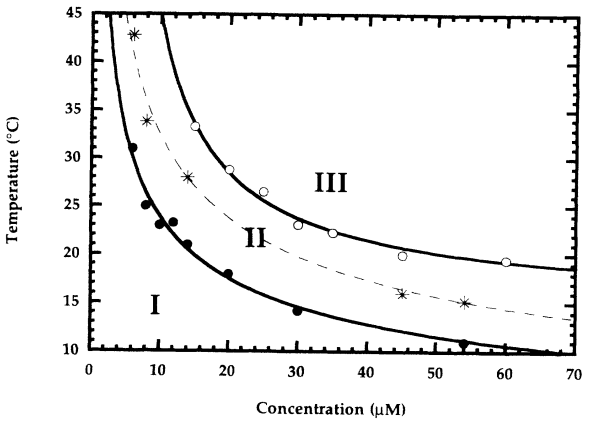

FIG. 2. The phase diagram of microtubule growth. I: region of no growth ($P_{occ} < \frac{1}{10}$). II: region of growth from nucleation sites ($P_{occ} > \frac{1}{10}$) The dotted line distinguishes between bounded growth (below) and unbounded growth (above). III: region of spontaneous nucleation. The lines are least-squares fits to the following function forms. (black dots): $T \sim C^{0.45}$; (stars): $T \sim C^{0.45}$; (open dots): $(T - T_c) \sim (C - C_c)^{-1}$, where $T_c = (15 \pm 1)$ °C and $C_c = (2 \pm 2)\,\mu M$.

crotubules. The fraction increases exponentially as the temperature rises, so there is no true onset for site nucleation. We define onset of site-nucleated growth when one microtubule is present for every 100 sites and plot this as the lowest curve in the phase diagram. Dynamic instability alone is not sufficient to explain such low levels of site occupation. There must be a barrier limiting the rate at which microtubules nucleate on empty sites to balance the rate at which microtubules dissemble completely.

As the temperature rises, site-nucleated microtubules increase in number and reach longer lengths. It has been predicted that the growth eventually becomes unbounded [12]. We present the first direct observations on this transition as the middle curve of the phase diagram.

Well above the transition to unbounded growth, microtubules nucleate spontaneously. We measure the density of microtubule ends as it increases steadily with time. The number of ends is indicative of the number of nucleation events. Thus we can determine the rate of nucleation and observe that it increases as the 12(±2)th power of the tubulin concentration. The onset of bulk nucleation (defined by practical considerations) is plotted as the uppermost curve of the phase diagram.

With this description of the phase diagram, we return to the regime of site nucleation and ask how the dynamics of individual microtubules reflect the transition from bounded to unbounded growth. From plots like Fig. 1, four parameters emerge as obvious measures of dynamic instability: two slopes, representing the rates of growing and shortening, and two time scales, representing the typical amounts of time spent in each state. The rate of growth is limited by the probability of sticking and increases as the temperature rises. The rate of shortening also increases at high temperatures. Altogether, higher temperatures favor assembly since the time spent growing gets longer and complete catastrophes occur less frequently.

Varying temperature and concentration permits a new approach to dynamic instability. By varying temperature we affect both growth and hydrolysis, but we can hold the velocity of growth constant with an appropriate change in the tubulin concentration. In this way, dynamic instability may be studied at different rates of GTP hydrolysis.

We observe that when the temperature is lowered and the growth velocity is held constant by increasing the tubulin concentration, length fluctuations are less frequent—a likely consequence of a slower rate of GTP hydrolysis. By probing low temperatures and high tubulin concentrations, we attempted to access a regime in which length fluctuations are suppressed altogether. Our efforts were not successful because the necessary concentration of tubulin ($> 100\mu M$) exceeds the limits set by the concentrations of GTP and Mg^{2+} in our buffer.

Throughout the experiment we notice that increases in temperature and concentration have qualitatively similar effects, raising the question of whether these two parameters are actually independent. It has been suggested [10b] that there may exist another state of tubulin aggregates (oligomers) that competes with microtubules, effectively lowering the concentration at low temperatures. We cannot rule out this possibility, but we can conclude that, were it true, essentially all the tubulin would have to be in oligomer form at low temperatures (~10 °C).

II. EXPERIMENTAL METHODS

Visualization. Our experimental setup, depicted in Fig. 3, is typical [13]. The central piece is a light microscope, equipped for differential-interference contrast (DIC). DIC microscopy must be pushed to its limits to make the signature of a microtubule visible. In particular, the resolution of the image must be extremely high. To this end, our microscope is equipped with a 63× oil-immersion ob-

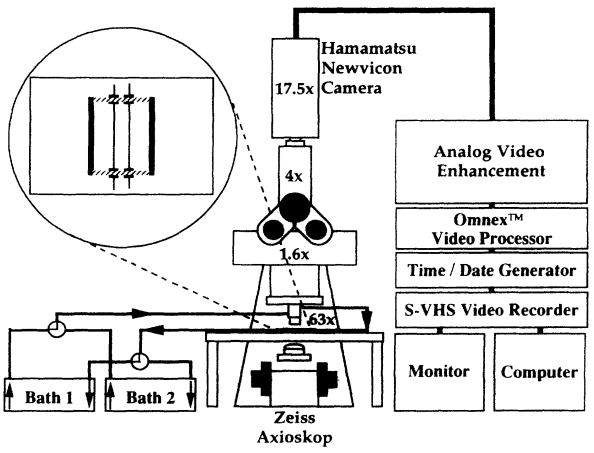

FIG. 3. A schematic of the experimental setup. The stages of magnification are labeled, beginning with the 63× objective and yielding a total magnification of 7056×. The magnified image is enhanced, processed, recorded, displayed, and analyzed. The blowup depicts the sample cell as described in the text. Interchange between two water baths allows rapid adjustment of the sample temperature.

jective of the largest available numerical aperture (1.4 NA) and a condenser of the largest numerical aperture possible without oil (0.9 NA). High resolution is achieved at the expense of contrast—the signature of a microtubule is too faint to be detected by eye. Thus a video camera is necessary. Adjustment of the gain and offset of the camera amplify the contrast of the image [14]. Digital image processing improves the image even further. We subtract a background image, average over two video frames, and apply a customized gray scale map, all in real time. In the final image, single microtubules are clearly visible and their ends are easily located. We record the video signal on tape.

Length measurement. To measure the length of individual microtubules, we use a Macintosh IIfx computer equipped with a Perceptics PixelPipeline frame-grabber card and a customized version of NIH Image video digitizer manager (VDM). The observer locates the position of one end of the microtubule on the computer screen with a cursor and clicks. The computer grabs a frame at the click, waits for a second click indicating the other end, saves the coordinates of the two ends and the time of the first click, and returns to live display. When the process is repeated, the result can be plotted as a time series, like the one shown in Fig. 1. The conversion from pixels into length (21 pixels /μm) is calibrated by substituting a precision stage micrometer (2 μm/division) for the specimen.

To accurately measure and track its length, it is best if the microtubule lies in the plane of focus and cannot float away. We achieve this in the standard way, by growing microtubules from nucleation sites stuck to the upper glass surface of the sample cell [15]. We limit the error associated with measuring projections by restricting our measurements to microtubules that have at least 10 μm lying in the plane of focus (depth < 1 μm). We measure the lengths of microtubules which do not fit in a single field of view (30 μm $\times 22.5$ μm) by referencing the fixed end to a speck on the glass surface and translating the sample while keeping the reference point in sight.

The systematic error in determining the length of microtubules which do not lie entirely in the plane of focus amounts to less than 1% of their actual length. The random error in a length measurement is ± 0.5 μm, estimated from scatter (the theoretical resolution limit is ± 0.25 μm), and is therefore the dominant error for microtubules less than 50 μm long. The error in the time measurement is easily restricted to ± 6 s (the observer response time), and can be ten times smaller if care is taken to analyze the video tape frame by frame.

Temperature control. To control the temperature of the specimen, it is necessary to control the temperature of the objective to which it is closely coupled through less than 100 μm of oil. We built a sleeve for the objective, and a holder for the sample, both with passages for fluid from a temperature controlled bath. The holder insulates the sample from air currents and prevents large thermal gradients. We use a dry (no oil) condenser in order to avoid controlling the temperature of the condenser. With a test sample containing a tiny thermocouple, we calibrated the temperature inside against the temperature of a resistance temperature detector (RTD) thermometer in the slide holder with an accuracy of ± 0.25 °C [16]. The sample temperature is stable over at least two hours and can be rapidly changed (15 °C/min) by switching between two baths, connected as shown in Fig. 3.

The remainder of this section contains a description of procedures aimed at controlling the chemical conditions of the sample. We are concerned with the *p*H of the solution, the concentrations of Mg^{2+} and GTP, and the concentration, purity, and integrity of the tubulin in solution. Purity and integrity are critical since small amounts of contaminating proteins or salts can have large effects. Furthermore, tubulin gradually "denatures" in vitro, meaning that it ceases to assemble into microtubules.

Lifetime. To estimate the lifetime of tubulin, we observed individual microtubules for long times at several different temperatures. Their dynamic instability is essentially unchanged after an hour at 37 °C but decays completely after 3 h. At lower temperatures, dynamic instability lasts longer—over 2 h at 18 °C. To minimize the effects of aging, we restrict our observation time to 30 min. We make exception to this rule when measuring the distribution of microtubule lengths for which longer times (~ 2 h) are necessary to determine whether a stationary state is achieved.

Purity. Ideally there should be no MAP's in the purified tubulin solution [9]. The Appendix contains a description of the procedure we follow to obtain tubulin in solution. To check the purity of our final solution we perform gel electrophoresis, which separates proteins based on their molecular weights, and silver staining, which reveals any protein present in an amount $\geq 10^{-9}$ g [17]. We find our solution is at least 99.9% (by weight) pure tubulin. Experiments [10(b)] indicate that the effect of MAP's on growth velocity and transition frequency become significant at levels near 1% (by weight).

Concentration. To determine the concentration of tubulin, we measure its absorption of 280- and 260-nm ultraviolet light. All proteins absorb in the ultraviolet because they contain amino acids with aromatic rings (tyrosine and tryptophan, in particular) [18]. Thus, the interpretation of an UV-absorption measurement in terms of concentration is only accurate for pure solutions. The measurement is slightly complicated by the fact that GTP also absorbs in the ultraviolet, albeit with a distinct spectrum.

The concentration of tubulin in our stock solution is 60 $\mu M \pm 2$ μM. We dilute to obtain other concentrations of tubulin. To minimize the errors involved in dilution, we make all samples of a desired concentration from a single dilution using fairly large volumes (≥ 100 μl). We estimate our errors from the accuracy of our pipetting to be $< 5\%$. When appropriate, axoneme fragments [11] are added during dilution. Samples (45 μl) of diluted solution are stored in liquid nitrogen until the beginning of a measurement.

The cell. At the beginning of a measurement, a cell is filled with a sample of tubulin solution and placed under the microscope. The cell is made of a "biologically-clean" glass microscope slide and coverslip [19], held 50 μm apart by a pair of tungsten wires, and sealed on two sides

and at the wires with 5-min epoxy, as illustrated in the blowup in Fig. 3. The cell is filled by capillary action and the open sides are then sealed with candle wax.

Tubulin can bind nonspecifically with the glass surfaces of the cell [18], changing the concentration in a potentially temperature dependent manner. The cell thickness represents the ratio of surface area to volume and, thus, the percent of tubulin lost to binding with the glass. To gain control over this unknown amount, we looked at how four different cell thicknesses (6, 12, 25, 50 μm) affected the formation of microtubules using 14-μM tubulin samples at 34 °C and 26 °C. The proportion of occupied nucleation sites P_{occ} is our most sensitive measure of tubulin concentration in situ (see Sec. III). We observed that P_{occ} was almost unchanged between 50 and 25 μm and decreased in the thinner cells (Fig. 4). Based on these observations, we use 50-μm-thick cells for all measurements.

Chemical conditions. We chose the chemical composition of the tubulin solution to be consistent with previous experiments on microtubules [10]. The solution contains between 6 and 60 μM tubulin, 1 mM GTP, 2 mM $MgSO_4$, 2 mM EGTA [ethylene glycol-bis (β-aminoethyl ether) N,N,N',N'-tetra acetic acid], and 100 mM Pipes buffer, at pH 6.9. Pipes is a standard buffer that works well near this pH. EGTA is a chemical that binds Ca^{2+} ions, which otherwise compete very effectively with Mg^{2+} ions for a binding site on tubulin and inhibit microtubule assembly. The concentrations of GTP and Mg^{2+} are well in excess of that of tubulin, with Mg^{2+} at a higher concentration to compensate for its strong association with GTP. We maintain these chemical conditions throughout the measurements, adjusting only the tubulin concentration.

History. The temperature history of a sample is of particular importance since microtubules can form at or below room temperature when a high concentration of tubulin is present. At the beginning of a measurement a room-temperature cell is filled with ice-cold tubulin solution, sealed with wax, and placed under the microscope. This process takes about 3 min. To erase any polymerization which may have occurred, the temperature is lowered to 4 °C for 10 min and then raised to the desired temperature (10–40 °C). After another 10 min equilibration time, observations begin.

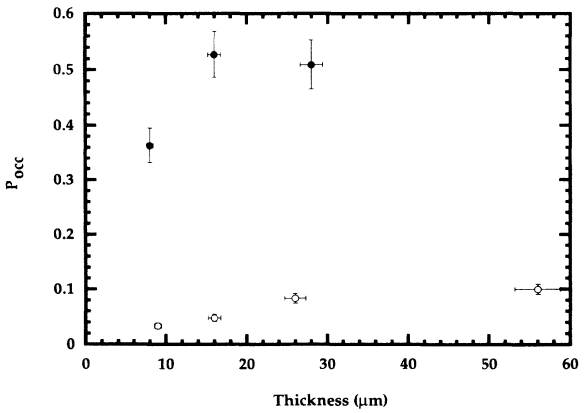

FIG. 4. P_{occ} vs sample thickness at two temperatures: 26 °C (open dots) and 34 °C (black dots).

III. RESULTS

A. Phase diagram

Site nucleation. At relatively low temperatures and tubulin concentrations, microtubules polymerize from nucleating sites. Under these conditions, the number of microtubules has a striking temperature dependence: over a range of temperatures only a fraction of the sites support a microtubule at any given time. This fraction is constant over at least an hour, though individual sites gain or lose microtubules. If the temperature is changed, a different constant proportion of the sites is occupied.

Figure 5 shows the proportion of nucleating sites occupied by a microtubule, P_{occ} = (number of microtubules)/(number of sites), as a function of temperature for four different concentrations. It is important to note that no distinction is made between the two types of nucleation sites [11]. Each measurement includes at least 1000 nucleating sites. The proportion of occupied sites increases exponentially with temperature. Since an exponential temperature dependence does not define an onset temperature, we arbitrarily define $P_{occ}=1/100$ as a practical onset and use it to plot the lower curve of the phase diagram. The measurement is not accurate for $P_{occ}>0.3$ due to the geometry of the nucleation sites [20]; however, qualitatively P_{occ} is observed to approach 1 at higher temperatures.

This behavior is very different from usual site-nucleation problems where, after some time, every nucleating site is occupied. Fractional occupation is a transient state with a lifetime determined by the activation energy needed to nucleate. Of course, if some sites are defective, a fractional occupation will arise, but it will not change with temperature or concentration. This is clearly not the case in the experiment described here (Fig. 5).

The steady-state fractional occupation of microtubule nucleating sites is a signature of dynamic instability. Since microtubules occasionally catastrophe (Fig. 1) and disappear completely, empty nucleating sites are constantly being "created." This process is balanced by the nucleation of new microtubules on empty sites, leading to a constant proportion of occupied sites. The proportion will reach unity only when microtubules never disassemble completely (i.e., rescue follows every catastrophe), and therefore grow on average. Fitting the temperature behavior of the occupation to the form

$$P_{occ}=e^{A(T-T_0)},$$

we can specify the temperature T_0 where $P_{occ}=1$ and know that above T_0 the microtubules will grow unbounded. We find $T_0 \sim C^{-1/2}$ and $A \sim C^{1/2}$ (see inset, Fig. 5).

Bounded-unbounded growth. The transition from bounded to unbounded growth, which had been predicted previously [12], can also be observed in the distribution of microtubule lengths. We catalogued the lengths of microtubules in four samples of 45-μM tubulin concentration at four different temperatures below 16 °C. Each

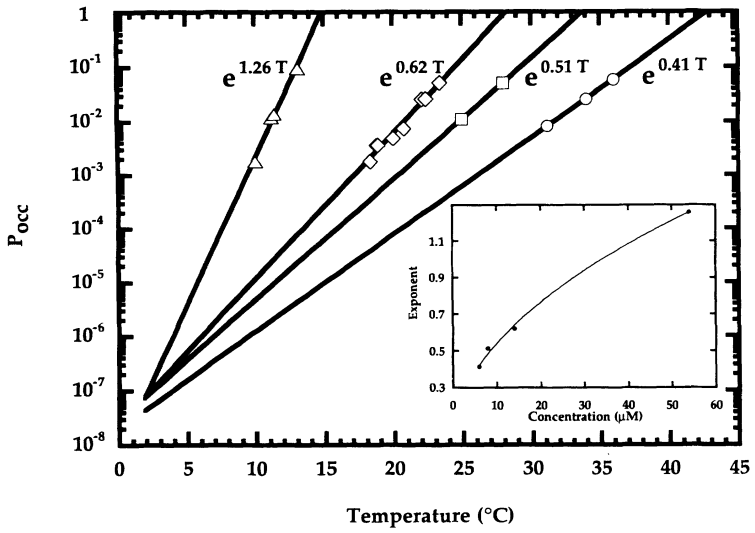

FIG. 5. The proportion of occupied sites (P_{occ}) vs temperature for four tubulin concentrations: 6 μM (dots); 8 μM (squares); 14 μM (diamonds); 54 μM (triangles). The lines are least-squares fits yielding the labeled exponents. The inset is a plot of the exponent vs the concentration. The solid line is a least-squares fit to the form exponent $\sim C^{0.5}$.

measurement lasted 2 h and the length distributions did not change in that time [21]. The histograms are shown in Fig. 6; the solid curves are least-squares fits to the exponential form

$$P(l) \sim e^{-l/l_0} .$$

The lowest bin at the two warmest temperatures was not included in the fits since the geometry of our nucleation sites introduces a bias against very short microtubules at high occupation levels ($P_{occ} > 0.3$) [20]. Elsewhere, the fits are very good. Since a stochastic process would lead to an exponential distribution of lengths, this result supports the hypothesis that dynamic instability is generated by a stochastic process.

Figure 7 is a plot of the characteristic length l_0, extracted from fits in Fig. 6, versus temperature. The solid curve is a least-squares fit to the functional form

$$l_0 \sim \left[1 - \frac{T}{T_0}\right]^{-1} .$$

This diverging length scale is the expected signature of unbounded growth. From the fit we find that T_0 (45 μM) $= 16.0 \pm 0.2$ °C. This transition temperature lies on the curve generated from the measurements of P_{occ} (middle curve, Fig. 2).

Above the transition, as expected, the length distribution is no longer stationary. The histograms for the first and second hour at 16.4 °C are shown in Fig. 8. The time dependence of the length distribution is evident in both the average and extreme lengths.

We do not observe the effects of depletion, where escaping microtubules screen the ones left behind from diffusing dimers [12]. Every microtubule enters the regime of unbounded growth at the same time. This can also be seen in the dynamics of individual microtubules, as described in Sec. III B.

Bulk nucleation. Microtubules can form spontaneously in the bulk. At temperatures and concentrations above the transition to unbounded growth, dynamic instability does not inhibit the growth of spontaneously nucleated microtubules. Of course, there is a potential barrier to spontaneous formation of a microtubule that must be overcome. Just above the transition to unbounded growth, the barrier is too high for any microtubules to appear in a reasonable time (< 5 h) and volume (a field of view). As temperature or concentration are increased, the probability of passing over the barrier increases sharply. We measure this probability by the time between the appearance of successive microtubules. The points on the upper curve of the phase diagram mark the conditions at which a new microtubule end appears in a $\sim 40\,000\ \mu m^3$ volume approximately every 5 min.

We measured how the nucleation time depends on tubulin concentration and temperature. Unlike usual first order transitions, the bulk nucleation of microtubules is not explosive. This reflects the fact that a microtubule is essentially a one-dimensional object. For this reason it is possible to measure the nucleation kinetics on a large range of temperatures and concentrations.

We have observed that the dependence on concentration follows a power law with an exponent of 12 ± 2 (Fig. 9). This is physically related to the microtubule structure, in particular the number of protofilaments [4]. A detailed discussion and model of the concentration and temperature dependence of this process will be given elsewhere [22].

It must be emphasized that our measurements up to this point have made no distinction between the two types of microtubule ends [4]. It is therefore possible that the transitions we describe actually come in pairs, one for each type of end. In our measurement of the onset of site nucleation, we cannot distinguish between the transitions of each end except to say that they must straddle the one we observe. We can say more about the transition from bounded to unbounded growth. Recall that we observed this transition in two different ways. First, the distribution of microtubule lengths becomes time dependent as soon as one of the two ends enters the unbounded regime. Second, we observe that at this transition to unbounded growth all of the nucleation sites are occupied, meaning that both ends are growing unbounded. Thus, to within

our temperature resolution, the two ends make the transition to unbounded growth together. Finally, the onset of bulk nucleation is far removed both in temperature and concentration from the bounded-unbounded transition. It is thus a single transition, determined by the kinetics of nucleation.

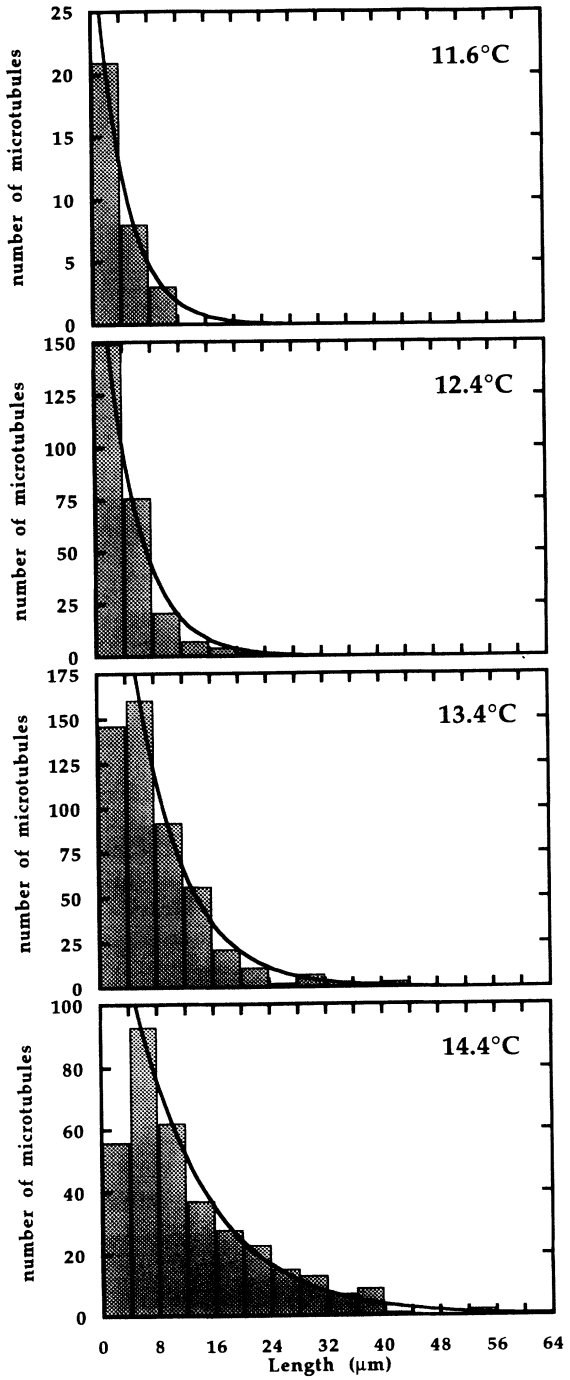

FIG. 6. Histograms of microtubule lengths at four different temperatures in the regime of bounded growth for 45-μM tubulin concentration. The lines are least-squares fits to the form $Ae^{(-l/l_0)}$. 11.6°C: $l_0 \sim (4.1 \pm 0.02)$ μm; 12.4°C: $l_0 \sim (4.8 \pm 0.5)$ μm; 13.4°C: $l_0 \sim (6.7 \pm 0.3)$ μm; 14.4°C: $l_0 \sim (10.5 \pm 0.5)$ μm.

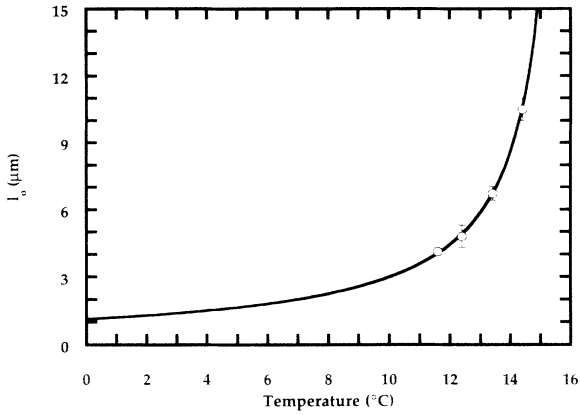

FIG. 7. The characteristic length l_0 vs temperature as measured from the histograms in Fig. 6. The line is a fit to the functional form: $P(l) \sim (1 - T/T_0)^{-1}$, where $T_0 = (16.16 \pm 0.05)$ °C.

B. Dynamical parameters

Having explored the phase diagram of microtubules in terms of properties of the microtubule population, we focus on the dynamics of individual microtubules. For simplicity, we restrict our discussion to data from the faster growing (plus) microtubule end and note that the slower growing (minus) end behaves similarly.

At three concentrations of tubulin (6, 14, and 45 μM)

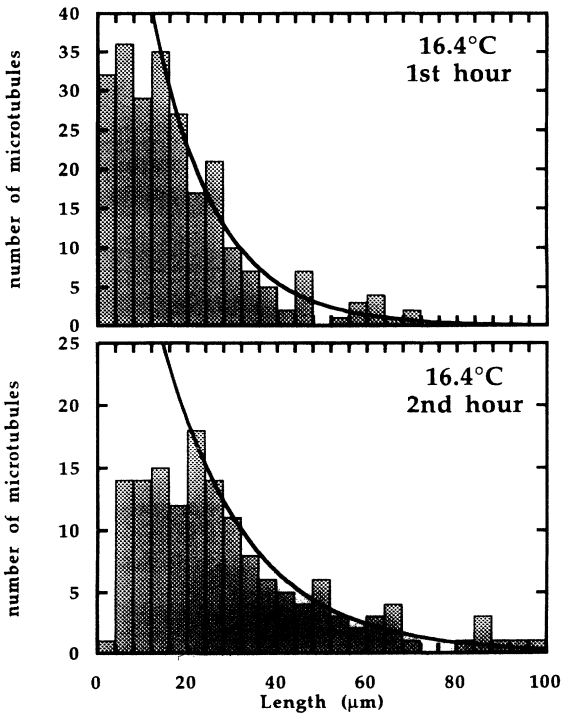

FIG. 8. Histograms of microtubule lengths during the first and second hours of observation at a temperature above the onset of unbounded growth (16.4 °C) for 45-μM tubulin concentration. The lines are least-squares fits as in Fig. 6. First hour: $l_0 \sim (14.0 \pm 1.5)$ μm; second hour: $l_0 \sim (19.3 \pm 1.7)$ μm.

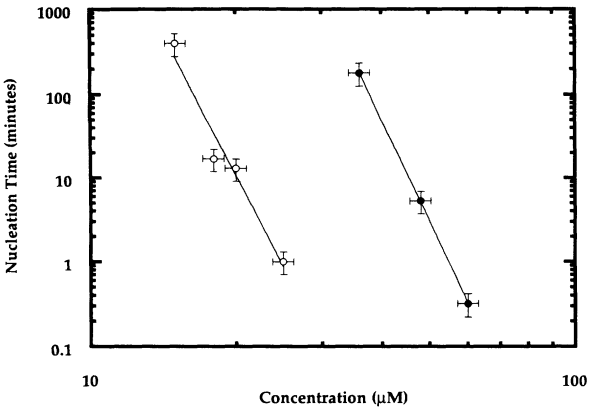

FIG. 9. The characteristic time for spontaneous nucleation in our experimental volume ($\sim 40\,000\ \mu m^3$) as a function of concentration at two temperatures: 30°C (open dots) and 20°C (black dots). The lines are least-squares fits to a power law. 30°C: $t \sim C^{11.3}$; 20°C: $t \sim C^{12.4}$.

and several different temperatures per concentration, we recorded the lengths of individual microtubules for up to 30 min, as illustrated in Fig. 1. We analyze the data in terms of four parameters: the velocity of growth V_g, the velocity of shrinking V_s, the time until catastrophe T_c, and the probability of rescue P_r.

V_g and V_s are the averages of least-squares fits to the positive and negative slopes in the time series, respectively. The individual slopes are weighted in the average by the fraction of the total time spent with each slope. Errors in these averages are ± 0.1 μm/min for V_g and ± 1 μm/min for V_s.

Velocity of growth. The velocity of microtubule growth can be thought of as the product of the rate R, at which dimers encounter the end of a microtubule and the probability P at which they stick. The rate of encounter can be calculated based on diffusion-limited transport. This calculation involves integrating the number of dimers a distance r from the microtubule end $n(r)$ divided by the time it takes a dimer to diffuse that distance $t(r)$ times the probability that a dimer diffuses in the direction of the microtubule end $p(r)$:

$$R = \int_a^\infty \frac{n(r)}{t(r)} p(r) dr = \int_a^\infty \frac{4\pi r^2 C}{r^2/D} \frac{\pi b^2}{4\pi r^2} dr = \frac{\pi b^2 DC}{a} ,$$

where a is the size of a dimer, b is the effective radius of a microtubule end, D is the diffusion constant, and C is the concentration of dimers.

Putting in reasonable values for these numbers ($D = kT/6\pi\eta a = 4\times 10^{-7}$ cm^2/sec; $C = 6\times 10^{15}$ dimers/cm^3; $b = 10^{-6}$ cm; $b/a = 2$), yields a rate of approximately 15 000 dimers/sec. Typical velocities of growth are about 30 dimers/sec (Fig. 10). Thus, the growth rate is limited by the probability that tubulin dimers stick to the microtubule and not by the rate at which they diffuse to the microtubule end [10(b)].

The velocity of growth increases significantly at higher temperatures. Two different mechanisms could cause this behavior. Either the probability of sticking is changing with temperature or there is a temperature controlled sink adjusting the effective concentration of tubulin dimers.

In the first case, we can apply our calculation of the rate of encounter to find the probability of sticking as a function of temperature. This is plotted in Fig. 10(c). Sticking probabilities are on the order of 2/1000 and change by a factor of 8 over a temperature range of 30°C. The curve is not a standard exponential form $e^{-B/kT}$, suggesting that the binding energy B is itself temperature dependent. This interpretation is plausible since the properties of water (e.g., viscosity, entropy) are changing over this temperature range.

In the case of the temperature controlled sink, we refer to the proposal that tubulin exists in an equilibrium between two forms, one that can assemble into microtu-

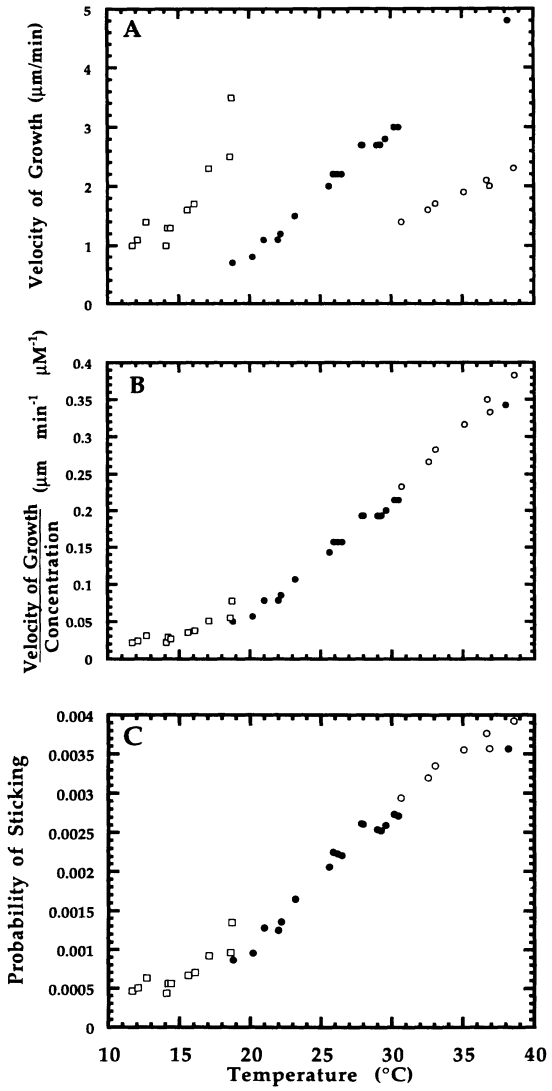

FIG. 10. (a) Velocity of growth vs temperature for three concentrations of tubulin: 6 μM (open dots); 14 μM (black dots); 45 μM (open squares). (b) Velocity of growth divided by tubulin concentration vs temperature. (c) Probability of sticking (as defined in the text) vs temperature.

bules (dimers) and another that cannot (oligomers) [10(b)]. Changes in temperature might shift this equilibrium, changing the effective concentration of dimers. Support for this argument comes from the existence of oligomers, which are more stable at lower temperatures [23].

The measurement of growth velocity spans a large range of tubulin concentration (Fig. 10). From the plot of velocity divided by total tubulin concentration [Fig. 10(b)] one can see that if it is assumed that no oligomers are present at 40 °C, then at 10 °C over 90% of the tubulin must be in oligomer form. While this seems implausible, it should be possible to test directly, perhaps using techniques of cryo-electron microscopy.

Velocity of shortening. Figure 11 is a plot of the velocity of shortening versus temperature for the three concentrations we investigated. The points lie on a single curve, indicating, as expected, that V_s is independent of concentration [10(c)]. Again the temperature effect is large, a factor of 8 over 30 °C. The similarity with the temperature dependence of the velocity of growth is remarkable and suggests that there may be a common effect involving a tubulin-microtubule-water interaction, which is sensitive to temperature.

Catastrophe. We measured the lifetime of the growing state in terms of the mean time until catastrophe T_c. This is calculated from the total time spent in the growing state (for all microtubules at a given temperature and tubulin concentration) divided by the total number of catastrophes observed. The calculation assumes an underlying random process, which is consistent with the results discussed above.

T_c is plotted as a function of temperature in Fig. 12(a). Its temperature dependence contains that of the velocity of growth. However, if the velocity of growth were the only relevant parameter, the points would collapse onto a single curve when plotted as a function of V_g. Figure 12(b) shows that this is not the case. We conclude that the rate of hydrolysis is also temperature dependent, such that lower temperatures (which correspond to higher concentrations in the figure) slow hydrolysis and extend the lifetime of the growing state.

There may exist a regime at low temperatures where catastrophes are suppressed altogether. However, the phase diagram indicates that to observe a reasonable number of microtubules at temperatures below 15 °C requires a very high concentration of tubulin. Once the tubulin concentration reaches 100 μM, special attention must be paid to the buffer conditions in order to provide an adequate excess of GTP and Mg^{2+}.

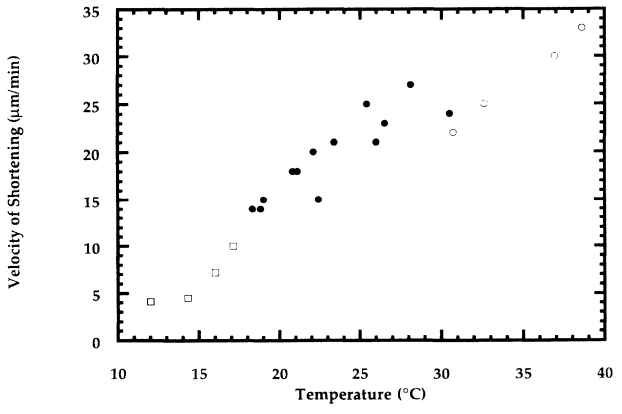

FIG. 11. Velocity of shortening vs temperature for three concentrations of tubulin: 6 μM (open dots); 14 μM (black dots); 45 μM (open squares).

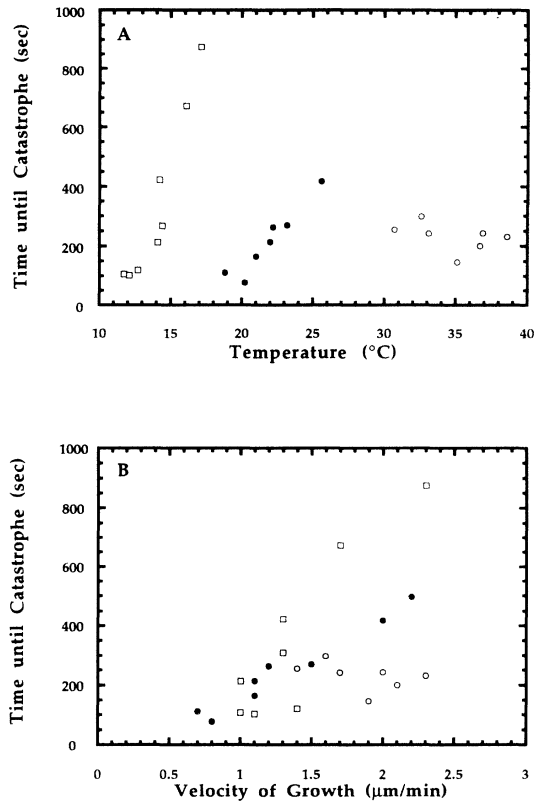

FIG. 12. (a) Time until catastrophe vs temperature for three concentrations of tubulin: 6 μM (open dots); 14 μM (black dots); 45 μM (open squares); (b) Time until catastrophe vs velocity of growth.

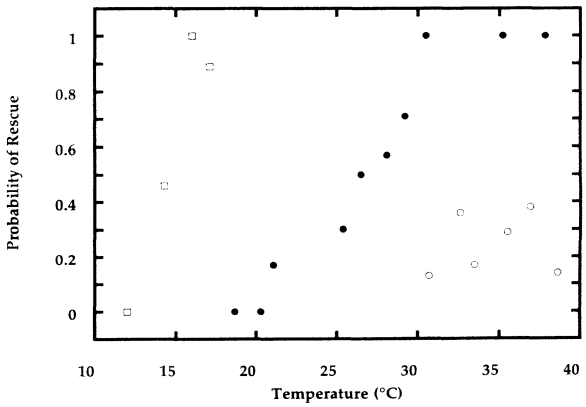

FIG. 13. Probability of rescue vs temperature for three concentrations of tubulin: 6 μM (open dots); 14 μM (black dots); 45 μM (open squares).

Rescue. The analysis of rescue events is complicated by the fact that microtubules occasionally disappear completely, biasing the calculation of a mean time spent shrinking towards shorter times. To extract more meaningful information, we define the probability of rescue P_r as the total number of rescues divided by the total number of catastrophes observed.

Figure 13 depicts the change in the probability of rescue as a function of temperature. Most noticeable is the fact that the probability of rescue reaches 1 at the temperature for the onset of unbounded growth.

IV. CONCLUSIONS

It is evident that microtubule assembly and dynamics are robust phenomena. They persist throughout a large range of temperatures and concentrations beyond the window of physiological relevance. This robustness indicates that the qualities of assembly measured throughout the phase diagram are relevant under biological conditions as well. Experiments that are difficult to control under physiological conditions because, for example, aging proceeds very quickly, can be performed at lower temperatures and referenced back to physiological conditions with confidence.

Several new aspects of microtubule growth have emerged. First, the stabilized microtubules in axonemes are not ideal nucleating sites. They do not grow immediately under favorable conditions, but rather present a sizable barrier to nucleating a microtubule. Related observations of a concentration dependent effect can be found in the literature [10(c)]. A more detailed investigation of the concentration dependence of this nucleation process should be performed to determine the number of tubulin dimers necessary to begin growth from a site.

Second, the addition of tubulin dimers to the end of a growing microtubule proceeds much slower than diffusion would allow. The temperature dependence of the growth velocity is not what the probability of sticking would suggest, indicating that the reaction kinetics are particularly sensitive to changes in the temperature. We plan to explore the role of water in these kinetics with measurements of the growth velocity as a function of the chemical potential of water.

Third, there is a sharp and robust transition from bounded to unbounded growth. This means that microtubules can be poised for a dramatic change in their assembly characteristics and a simple switch (possibly a MAP) would be all that is necessary to regulate microtubule behavior.

Finally, microtubule length statistics support the hypothesis that a stochastic mechanism underlies dynamic instability. We have, however, noted an apparent correlation between consecutive rescue sites. We plan to document this correlation more carefully. Perhaps MAP's or structural defects are key elements in the assembly dynamics.

Dynamic instability aside, microtubules are remarkable in that they can assemble spontaneously in the bulk. Effectively one-dimensional crystals, microtubules are an ideal system in which to study the phenomenon of bulk nucleation. Their restricted dimensionality implies that the transition, though sharp, is not explosive. Thus, with microtubules, bulk nucleation can be studied over a greater range than is usually possible. We have already begun experiments to understand and model this phenomenon in greater detail.

ACKNOWLEDGMENTS

Ted Salmon, Gerry Waters, and their students were generous with their time and resources. Robely Williams and Tim O'Brien provided patient explanations and encouragement. Adam Simon helped with the protein purification and Andreas Tilgner customized the software we use. Steven Grossman assisted in data collection and analysis. We are also indebted to Marileen Dogterom, Henrik Flyvbjerg, Tim Holy, Stanislas Leibler, and Kim Sneppen for insightful discussions.

APPENDIX

We use the a standard protocol for purifying tubulin [24]. We isolate tubulin from mammalian (bovine) brain. First, the brain is homogenized in a blender. The homogenate is repeatedly centrifuged to separate the material by weight. The centrifugation procedure takes advantage of the general temperature dependence of microtubule polymerization. By successively saving the material that is lightest at low temperatures (4 °C) and heaviest at high temperatures (37 °C) through three temperature cycles, we refine the mixture to the point of containing only tubulin and MAP's [9]. The MAP's are removed by adjusting the *p*H of the solution to the iso-electric point of tubulin (*p*H 6.7) and passing the solution through a column of a phosphocellulose ion exchanger. Tubulin is neutral at this *p*H, but MAP's are charged and therefore bind strongly to the phosphocellulose. The tubulin passing through the column loses its GTP and Mg^{2+} as well as the MAP's. These two chemicals must be added immediately to the eluted solution to stabilize tubulin in its native conformation. A final cycle of warm-cold centrifugation is then performed to remove any tubulin that denatured while passing through the column. The purified tubulin solution is stored in small vials (~ 500 μl/vial) in liquid nitrogen (77 °K). It can be stored this way for at least a year without denaturing. Storage in separate small amounts minimizes the number of times the tubulin is thawed and refrozen. Step-by-step protocols have been published [24] or are available upon request from the authors.

---

[1] Tubulin is actually the generic name of several nearly identical globular proteins individually referred to with the prefix α, β, or γ. Most tubulin in nature exists as a heterodimer of one α-tubulin and one β-tubulin molecule (molecular weight $\sim 110\,000$ daltons). For the purposes of this paper, the name tubulin refers to this heterodimer. The dimer is approximately 40-Å wide and 80-Å long.

[2] α and β tubulin each associate with a molecule of GTP: α

tubulin binds GTP nonexchangeably while β tubulin binds GTP exchangeably with an affinity that depends on the concentration of Mg^{2+}. R. C. Weisenberg, G. G. Borisy, and E. W. Taylor, Biochemistry **7**, 4466 (1968); J. J. Correira, L. T. Bary, and R. C. Williams, J. Biol. Chem. **262**, 17278 (1987).

[3] The attraction between tubulin dimers comes from weak intermolecular interactions such as hydrophobic and van der Waals interactions.

[4] The microtubule has a crystalline organization. Tubulin dimers align head to tail in parallel protofilaments, lining the wall of the microtubule. There are typically 13 protofilaments. Neighboring protofilaments are offset by ~ 9 Å, creating a pattern of three intertwined helices. The microtubule is a polar structure: one end (known as the minus end) exposes only α tubulin and the other (the plus end) exposes only β. E. M. Mandelkow, R. Schultheiss, R. Rapp, M. Müller, and E. Mandelkow, J. Cell. Biol. **102**, 1067 (1986); D. Chrétien and R. H. Wade, Biol. Cell. **71**, 161 (1991); T. J. Mitchison, Science **261**, 1044 (1993).

[5] B. Alberts, D. Bray, J. Lewis, M. Raff, K. Roberts, and J. D. Watson, *Molecular Biology of the Cell,* 2nd ed. (Garland, New York, 1989), Chap. 10; J. Darnell, H. Lodish, and D. Baltimore, *Molecular Cell Biology,* 2nd ed. (Freeman/Scientific American, New York, 1990), Chap. 21.

[6] T. Mitchison and M. Kirschner, Nature **312**, 232 (1984); **312**, 237 (1984).

[7] R. A. Walker, S. A. Inoué, and E. D. Salmon, J. Cell Biol. **108**, 931 (1989); R. A. Walker, N. K. Pryer, and E. D. Salmon, J. Cell Biol. **114**, 73 (1991); W. A. Voter, E. T. O'Brien, and H. P. Erickson, Cell Motility Cytoskeleton **18**, 55 (1991); A. A. Hyman, S. Salser, D. N. Dreschel, N. Unwin, and T. J. Mitchison, Mol. Biol. Cell **3**, 1155 (1992); M. R. Mejillano, J. S. Barton, and R. H. Himes, Biochem. Biophys. Res. Commun. **166**, 653 (1990).

[8] M. Caplow, Current Opinion Cell Biol. **4**, 58 (1992); H. P. Erickson and E. T. O'Brien, Annu. Rev. Biophys. Biomol. Struct. **21**, 145 (1992).

[9] Certain proteins, known as microtubule-associated proteins (MAP's), bind to microtubules in the cell and modify dynamic instability.

[10] (a) E. T. O'Brien, E. D. Salmon, R. A. Walker, and H. P. Erickson, Biochem. **29**, 6648 (1990); (b) D. N. Dreschel, A. A. Hyman, M. H. Cobb, and M. W. Kirschner, Mol. Biol. Cell **3**, 1141 (1992); (c) R. A Walker, E. T. O'Brien, N. K. Pryer, M. F. Soborio, W. A. Voter, H. P. Erickson, and E. D. Salmon, J. Cell. Biol. **107**, 1437 (1988).

[11] We use axoneme fragments to nucleate microtubules. Axonemes are the backbone structure of flagella [5]. They are a bundle of 11 microtubules, 9 so-called doublet microtubules in a circle around two single microtubules, stabilized and held together by other proteins. Thus each axoneme fragment contains 22 nucleating sites, 11 plus ends on one side, and 11 minus ends on the other [4]. Our particular axonemes come from the sperm of sea urchins from the laboratory of Professor E. D. Salmon. A protocol for isolating axoneme fragments is given in Ref. [10(c)].

[12] M. Dogterom and S. Leibler, Phys. Rev. Lett. **70**, 1347 (1993).

[13] B. J. Schnapp, Methods Enzymol. **134**, 561 (1986).

[14] S. A. Inoué, *Video Microscopy* (Plenum, New York, 1986).

[15] It should be noted that there is no significant effect of the glass surface on microtubule growth, because growth is a slow process as compared to diffusion. Solving the diffusion equation for typical tubulin concentrations and microtubule growth rates leads to a characteristic depletion length $l_D = \omega/4\pi DC \sim 10$ Å, where ω is the number of monomers sticking to the microtubule end per unit time (1625/min), D is the diffusion constant for tubulin dimers (4×10^{-7} cm^2/sec), and C is the concentration of tubulin dimers ($\sim 10\,\mu M$).

[16] We use a type E thermocouple with 13-μm wires and a platinum RTD from Omega Engineering.

[17] B. D. Hames in *Gel Electrophoresis of Proteins: A Practical Approach,* 2nd ed., edited by B. D. Hames and D. Rickwood (Oxford University Press, Oxford, 1990).

[18] R. K. Scopes, *Protein Purification: Principles and Practice,* 2nd ed. (Springer-Verlag, New York, 1987).

[19] D. A. Lutz and S. A. Inoué, Meth. Cell Biol. **37**, 89 (1986).

[20] The nucleation sites are arranged such that 11 sites are close together [14]. While competition between sites is not a factor [15] when more than four microtubules are growing on the same axoneme end, shorter microtubules are not visible among the stalks of the longer ones.

[21] We determined that the distributions were static by splitting the lengths into two one-hour intervals and comparing the histograms.

[22] D. Kuchnir Fygenson, *et al.* (unpublished).

[23] R. Melki, M.-F. Carlier, D. Pantaloni, and S. N. Timasheff, Biochem. **28**, 9143 (1989).

[24] R. C. Williams in *The Cytoskeleton: A Practical Approach,* edited by K. L. Carraway and C. A. C. Carraway (Oxford University Press, New York, 1992).

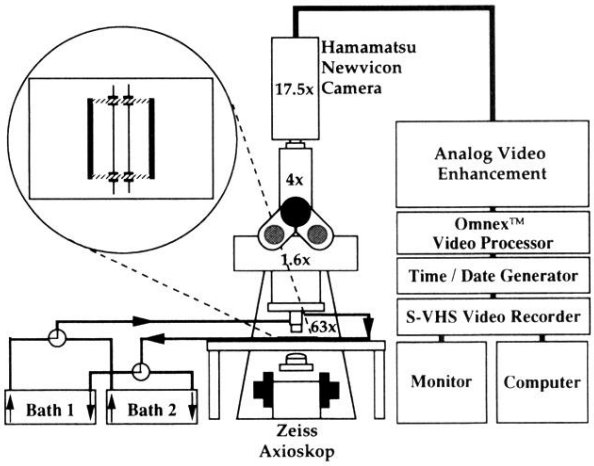

FIG. 3. A schematic of the experimental setup. The stages of magnification are labeled, beginning with the 63× objective and yielding a total magnification of 7056×. The magnified image is enhanced, processed, recorded, displayed, and analyzed. The blowup depicts the sample cell as described in the text. Interchange between two water baths allows rapid adjustment of the sample temperature.

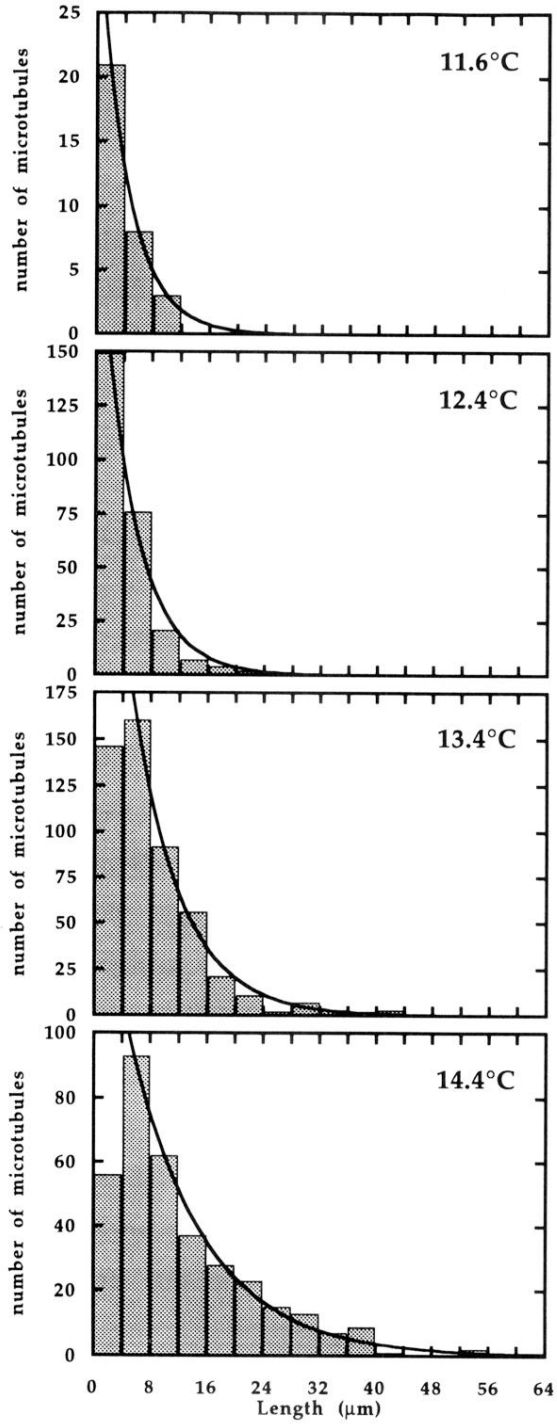

FIG. 6. Histograms of microtubule lengths at four different temperatures in the regime of bounded growth for 45-μM tubulin concentration. The lines are least-squares fits to the form $Ae^{(-l/l_0)}$. 11.6°C: $l_0 \sim (4.1 \pm 0.02)$ μm; 12.4°C: $l_0 \sim (4.8 \pm 0.5)$ μm; 13.4°C: $l_0 \sim (6.7 \pm 0.3)$ μm; 14.4°C: $l_0 \sim (10.5 \pm 0.5)$ μm.

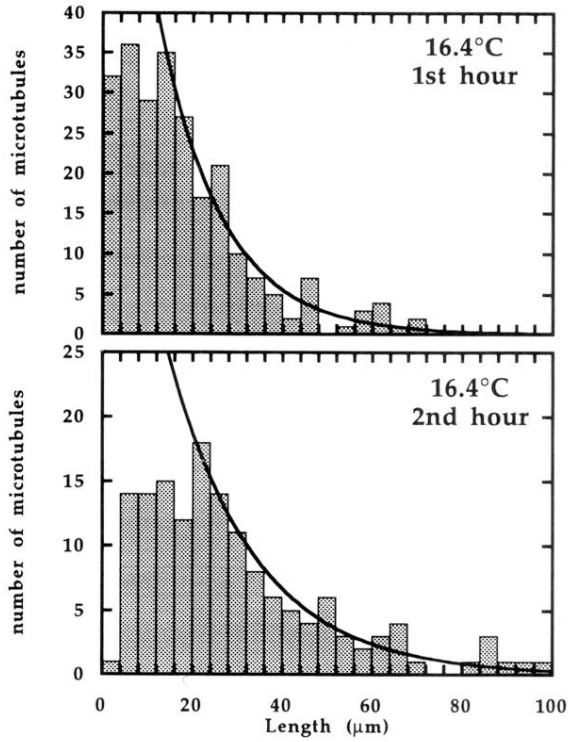

FIG. 8. Histograms of microtubule lengths during the first and second hours of observation at a temperature above the onset of unbounded growth (16.4 °C) for 45-μM tubulin concentration. The lines are least-squares fits as in Fig. 6. First hour: $l_0 \sim (14.0 \pm 1.5)\ \mu$m; second hour: $l_0 \sim (19.3 \pm 1.7)\ \mu$m.